Electrochemical Performance of Sn_4P_3 Negative Electrode for Na-Ion Batteries in Ether-Substituted Ionic Liquid Electrolyte

Kazuki Yamaguchi[a,b], *Hiroyuki Usui*[a,b], *Yasuhiro Domi*[a,b], *Haruka Nishida*[a,b], *Takuro Komura*[a,b], *Toshiki Nokami*[a,b], *Toshiyuki Itoh*[a,b], and *Hiroki Sakaguchi*[a,b,*]

[a]Department of Chemistry and Biotechnology, Graduate School of Engineering, and [b]Center for Research on Green Sustainable Chemistry, Tottori University, 4-101 Minami, Koyama-cho, Tottori 680-8552, Japan

[*]**Corresponding Author**

Tel/Fax: +81-857-31-5265, E-mail: sakaguch@tottori-u.ac.jp

Keywords: Tin phosphide; Na-ion battery; Ionic liquid electrolyte; Ether-substitution

Abstract

We have previously disclosed that the ionic-liquid electrolyte sodium bis(fluorosulfonyl)amide (NaFSA)/1-methyl-1-propylpyrrolidinium bis(fluorosulfonyl)amide (Py13-FSA) can significantly improve the cycling stability of Sn_4P_3 negative electrodes for Na-ion batteries (NIBs). However, the strong electrostatic interaction between Na^+ and FSA^- in the electrolyte leads to high viscosity and low conductivity. In this study, we have tried to improve the conductivity of the electrolyte and enhance the rate capability of the Sn_4P_3 electrode by introducing an ether group in the side-chain of the ionic liquid cation to reduce said electrostatic interaction. Ether-substituted ionic liquid 1-methoxymethyl-1-methylpyrrolidinium (PyMOM)-FSA showed higher conductivity than Py13-FSA and the Sn_4P_3 electrode exhibited a higher rate capability. The differential capacity vs. potential plots suggest that the reaction between Na^+ and Sn or P is promoted in the ether-substituted ionic liquid electrolyte. These results demonstrate that introduction of an ether moiety is an effective approach to improve the rate capability of the Sn_4P_3 electrode in NIBs.

1. Introduction

Na-ion batteries (NIBs) have attracted much attention as large-scale stationary batteries as Na resources are ubiquitous in seawater and earth's crust.[1] As a negative-electrode material for NIBs, hard carbon is a promising active material, which can store Na^+ in its nanopores and interlayer space.[1] A hard carbon negative electrode has been reported to exhibit a reversible capacity of *ca*. 350 mA h g^{-1}.[2] On the other hand, Na-ion capacitors (NICs) are also prospective energy-storage devices, negative electrodes for NIBs can be applied their negative electrodes.[3] Wang *et al.* revealed that mesoporous Nb_2O_5/carbon nanofiber composite negative electrode for NICs showed excellent rate capability with 171.4 mA h g^{-1} even at current density of 30,000 mA g^{-1}[4]. Nevertheless, active materials for negative electrode with higher capacity have been desired to further increase the energy density of NIBs and NICs. Thus, many researchers have intensively explored metal- and alloy-based active materials: Sn,[5] P,[6] and Sb,[7] have been reported to name a few. In this context, we have reported for the first time SiO[8] and SnO[9] as active materials for NIBs. Among them, P has the highest theoretical capacity of 2600 mA h g^{-1} (Na_3P), although it exhibits poor cycling stability due to its large volumetric change of 490% during the sodiation–desodiation reaction.[10] To improve the poor cyclability of P electrodes, composite materials have been proposed. For example, Shimizu *et al*. developed Ni-coated P particles via an electroless deposition method. A Ni-coated P electrode exhibited a capacity of 780 mA h $g(P)^{-1}$ even after 60 cycles.[11] On the other hand, we have developed a variety of phosphides (Sn–P,[12–14] Ge–P, Si–P, Cu–P, In–P, La–P[15]) and investigated their sodiation–desodiation properties. As a result, the Sn_4P_3 electrode was found to exhibit the best cycling performance with a high capacity of 750 mA h g^{-1} that was maintained over 200 cycles.[13]

The electrolyte is one of the most important components determining the cycle life and safety of batteries. The safety requirements increase with the energy density of the batteries. Thus, non-flammable ionic liquids are a promising alternative to conventional organic electrolytes.[16] Li *et al*. applied an ionic liquid electrolyte of sodium bis(fluorosulfonyl)amide (NaFSA)/1-methyl-1-propylpyrrolidinium bis(fluorosulfonyl)amide (Py13-FSA) to a Sb_2S_3/graphene electrode, and reported a reversible capacity of *ca*. 600 mA h g^{-1} over 100 cycles.[17] They showed also non-flammability of the electrolyte by testing with an electric Bunsen burner.[17] We have also firstly demonstrated that this ionic liquid electrolyte is effective to enhance the safety of NIBs by using a closed-system fire-resistance evaluation.[6,18] Moreover, the Sn_4P_3 electrode was found to exhibit superior performance in NaFSA/Py13-FSA than in a conventional carbonate-based electrolyte.[12,13]

In general, since Na^+ is coordinated by solvent molecules in the electrolyte, it inserts in the negative-electrode material via a desolvation process during charging. The charge density of Na^+ is smaller than that of Li^+, resulting in an easier desolvation process for Na^+. Nonetheless, the strong electrostatic interaction of Na^+ with FSA^- in the ionic liquid electrolyte hinders the Na^+ transport, not only at the electrode–electrolyte interface but also in the electrolyte bulk. In the case of Li-ion batteries (LIBs), we have demonstrated that the capacity of Si-based electrodes is significantly promoted by introducing an ether group, *e.g.*, methoxyethoxymethyl (MEM), in the side-chain of the ionic liquid cation.[19] The local negative charge of the oxygen atom in the ether group weakens the interaction between the Li^+ and bis(trifluoromethanesulfonyl)amide (TFSA) ions, enabling smooth Li^+ transport at the electrode–electrolyte interface. Therefore, we envisioned that the introduction of an ether group in the cation side-chain would enhance the electrochemical performance in NIBs as well. However, MEM is a relatively long chain, which

results in higher viscosity and lower conductivity.[20] In this study, we tried to achieve smooth Na^+ transport at the electrode–electrolyte interface, as well as in the electrolyte bulk, by introducing an oxygen atom in the Py13 cation with a shorter side-chain compared to that of the 1-((2-methoxyethoxy)methyl)-1-methylpyrrolidinium (Py1MEM) cation.

2. Experimental

Figure 1 shows the cation and anion structures of the ionic liquids used in this study. Two ionic liquids were synthesized by a previously reported organic method:[21] 1-methoxymethyl-1-methylpyrrolidinium bis(fluorosulfonyl)amide (Py1MOM-FSA) and 1-((2-methoxyethoxy)methyl)-1-methylpyrrolidinium bis(fluorosulfonyl)amide (Py1MEM-FSA). Py13-FSA was purchased from Kanto Chemical Co., Inc., and used without further purification. We confirmed the water content of the ionic liquids to be <50 ppm on a Karl Fischer moisture titrator (Labconco Corporation, FZ-Compact). Ionic liquid electrolytes were prepared by dissolving NaFSA in each ionic liquid with a concentration of 1 mol dm^{-3} (M). The conductivity was evaluated by electrochemical impedance measurements (CompactStat, Ivium Technologies) using a cell equipped with two Pt electrodes under Ar atmosphere at temperatures ranging from 298 to 333 K.

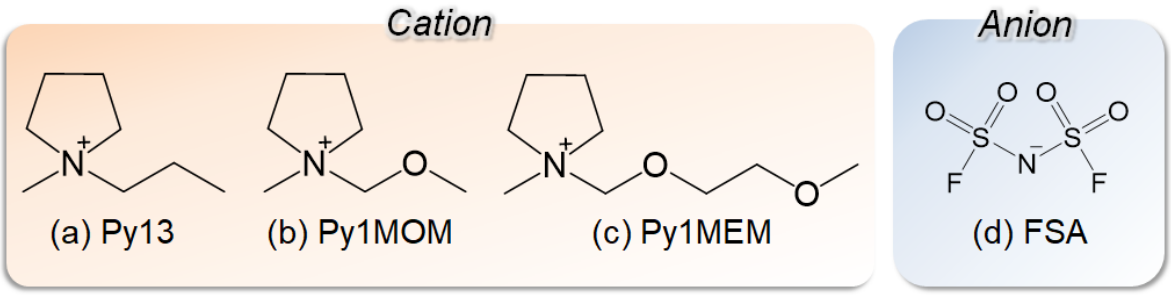

Figure 1 Chemical structure of (a) 1-methyl-1-propylpyrrolidinium (Py13), (b) 1-methoxymethyl-1-propylpyrrolidinium (Py1MOM), (c) 1-((2-methoxyethoxy)methyl)-1-propylpyrrolidinium (Py1MEM), and (d) bis(fluorosulfonyl)amide (FSA).

The Sn_4P_3 active material powder was synthesized by mechanical alloying (MA) using tin powder (99.99%, Rare Metallic) and red phosphorus powder (99.8%, FUJIFILM Wako Pure Chemical Corporation) as the raw materials. The detailed conditions have been described elsewhere.[13] Sn_4P_3 powder (70 wt%) was mixed with acetylene black (15 wt%), carboxymethyl cellulose (10 wt%), and styrene-butadiene rubber (5 wt%). The resulting slurry was uniformly coated on an Al foil with 20 μm thickness. Then, the electrode was punched with holes of $\phi = 1.0$ cm. The mass loading and thickness of the active material layer were approximately 1.2 mg cm^{-2} and 10 μm, respectively. We assembled a 2032-type coin cell consisting of a Sn_4P_3 working electrode, glass fiber separator, and Na foil counter-electrode. Charge–discharge tests were performed using an electrochemical measurement system (HJ-1001 SD8, Hokuto Denko Co., Ltd.) in the potential range between 0.005 and 2.000 V vs. Na^+/Na at 303 K under current densities from 50 to 10000 mA g^{-1} (corresponding to 0.04–8.83C), since the theoretical capacity of Sn_4P_3 is 1133 mA h g^{-1}. The interactions between Na^+ and FSA^- in the ionic liquid electrolytes were analyzed on a Raman microscopy system (NanofinderFLEX, Tokyo Instruments, Inc.) using the 532 nm line of a Nd:YAG laser through a 50-power objective

lens at *ca.* 298 K. To avoid the effect of the moisture in air, we placed the electrolyte solution into a quartz cell and tightly sealed it under Ar atmosphere.

3. Results and Discussion

Figure 2 shows the temperature dependence of the conductivity of the different ionic liquid electrolytes. The conductivities of NaFSA/Py13-FSA, NaFSA/Py1MEM-FSA, and NaFSA/Py1MOM-FSA at 303 K were 5.66, 3.95, and 7.11 mS cm^{-1}, respectively. NaFSA/Py1MOM-FSA exhibited higher conductivity than NaFSA/Py13-FSA. This is attributed to the electron donation from the methoxy group to the Py1MOM cation center to counter the positive charge.[22] Consequently, the electrostatic interaction between $Py1MOM^+$ and FSA^- is weakened and the conductivity increases. Although Py1MEM-FSA bears a MEM group with electron-donation ability, its conductivity was the lowest of all the ionic liquid electrolytes tested. This is attributed to the long side-chain of the cation.[20] Therefore, both the short side-chain and electron-withdrawing group contribute to the improved conductivity of Py1MOM-FSA. Activation energies of 1 M NaFSA/Py13-FSA, Py1MOM-FSA, and Py1MEM-FSA were 22.6, 19.9, and 23.7 kJ mol^{-1}, respectively. Thus, the conductivity of 1 M NaFSA/Py1MOM-FSA has lower temperature dependence compared to that of the other electrolytes, which should be advantageous for operation at low temperature.

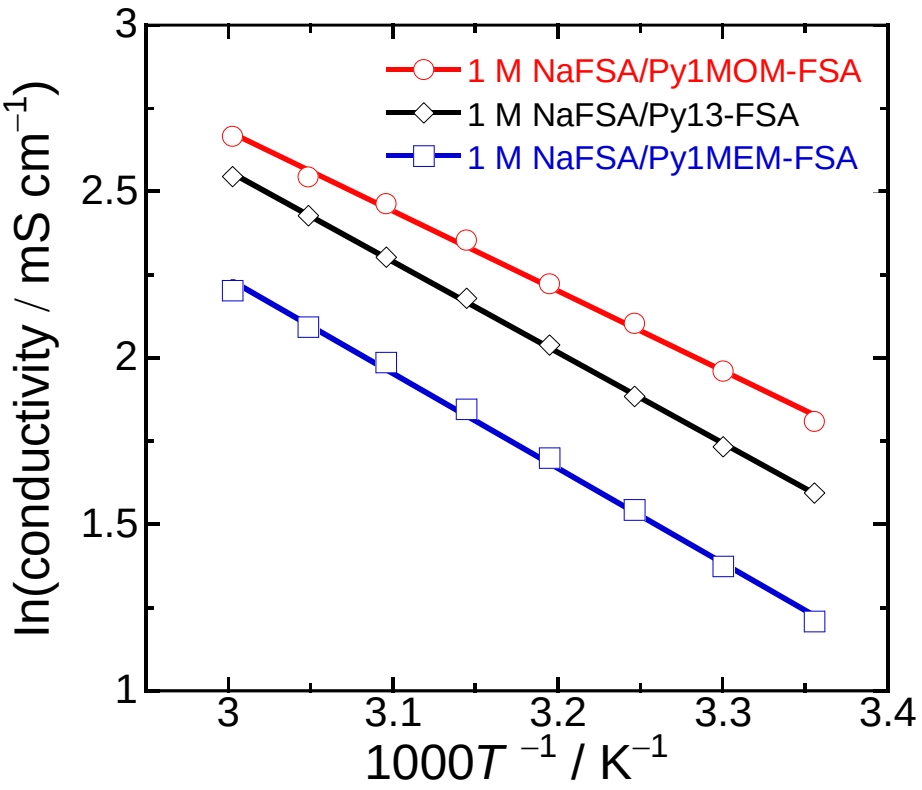

Figure 2 Temperature dependence of the conductivity of the pyrrolidinium-based ionic-liquid electrolyte solutions.

Higher conductivity of the electrolyte should lead to higher rate capability; thus, the Py1MOM-based electrolyte should be able to improve the rate capability of Sn_4P_3 electrodes. We performed rate-capability tests for a Sn_4P_3 negative electrode in these ionic liquid electrolytes (Figure 3). Discharge capacities of 660 and 240 mA h g^{-1} were obtained in the Py13-based electrolyte at current densities of 50 and 1000 mA g^{-1}, respectively. Although the conductivity of the Py1MEM-based electrolyte was the lowest, the electrode exhibited higher rate capability than in the Py13-based electrolyte: capacities of 850 and 290 mA h g^{-1} were measured at current densities of 50 and 1000 mA g^{-1}, respectively. In the Py1MOM-based electrolyte, the electrode

showed the best rate capability, maintaining a discharge capacity of 360 mA h g^{-1} even at 1000 mA g^{-1}, thus surpassing the capacity of hard carbon negative electrodes. By decreasing the current rate to 50 mA g^{-1} in the 51st cycle, the capacities were largely recovered in all the electrolytes. Thus, the capacity fading at high current densities might not be caused by electrode disintegration. As expected, the Py1MOM-based ionic liquid electrolyte enhanced the rate capability of the Sn_4P_3 electrode at current densities up to 2000 mA g^{-1}. However, no differences in the performance were observed at current densities over 2000 mA g^{-1}. We have previously confirmed that the Sn_4P_3 electrode exhibits a reversible capacity of *ca.* 250 mA h g^{-1} even at 3000 mA g^{-1} in the Py13-based electrolyte at 333 and 363 K.[14] Thus, the low capacities at high current densities over 2000 mA g^{-1} must be caused by slow Na^+ diffusion in the Sn_4P_3 active material layer. The Py1MEM-based electrolyte was also found to enhance the performance of the electrode compared to the Py13-based electrolyte. It was thus concluded that not only high conductivity is required to improve the rate capability. To clarify the factors enhancing the rate capability, we focused on the charge–discharge behavior of the Sn_4P_3 electrode in the different electrolytes.

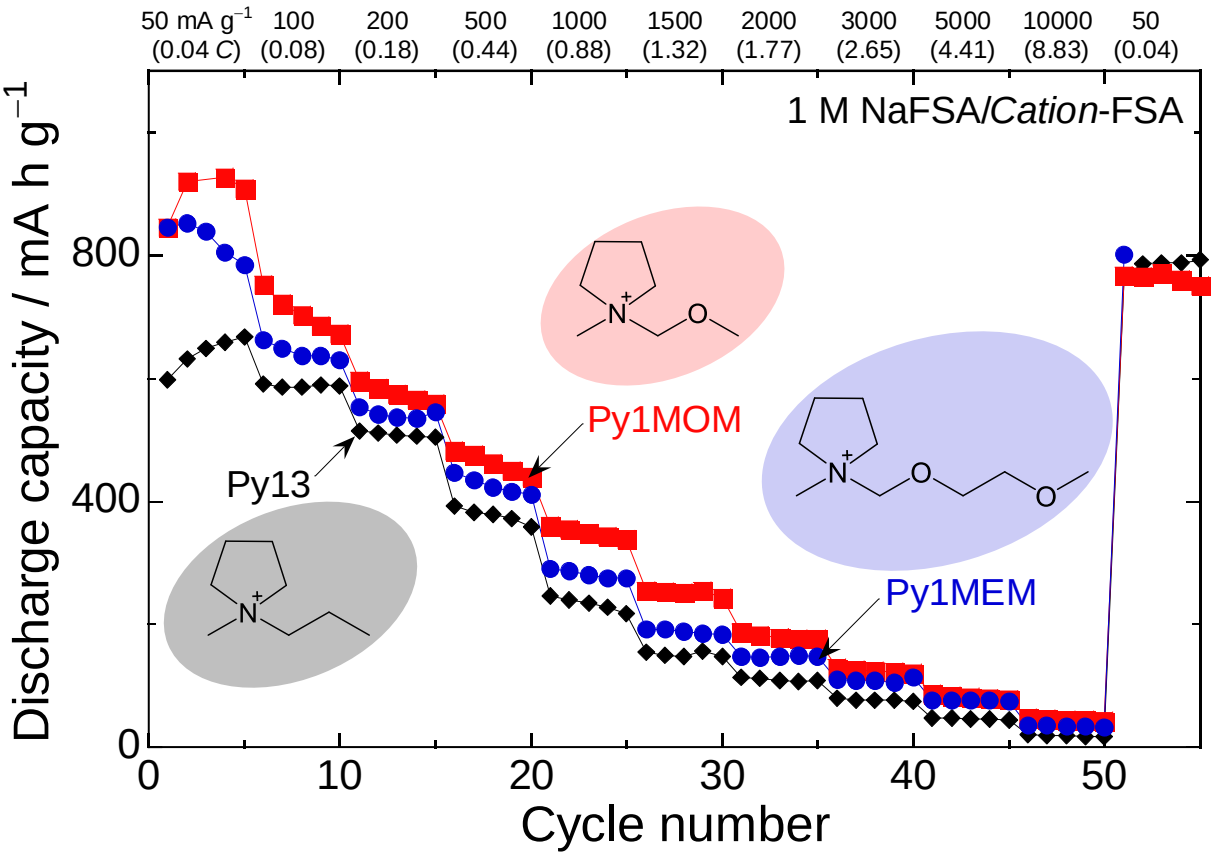

Figure 3 Rate capability of the Sn_4P_3 electrode in 1 M NaFSA dissolved in Py1MOM-FSA, Py1MEM-FSA, and Py13-FSA.

Qian *et al*. and Kim *et al*. have reported that Sn_4P_3 phase separation occurs at the first cycle to form elemental Sn and P, and that Sn and P individually react with Na^+ in subsequent cycles.[23,24] We have also confirmed the following reaction mechanism by transmission electron microscopy analysis:[13]

At the first charge (sodiation):

$$Sn_4P_3 + 24Na^+ + 24e^- \rightarrow Na_{15}Sn_4 + 3Na_3P \quad (1)$$

Subsequent cycles:

$$P + 3Na^+ + 3e^- \rightleftarrows 3Na_3P \quad (2)$$

$$4Sn + 15Na^+ + 15e^- \rightleftarrows Na_{15}Sn_4 \quad (3)$$

Figure 4a, c, and e shows the charge–discharge curves of the Sn_4P_3 electrodes in the Py1MOM-, Py1MEM-, and Py13-based ionic liquid electrolytes, respectively. In all the electrolytes, potential plateaus are observed at 0.1 V vs. Na^+/Na on the charge curve and at 0.2 V vs. Na^+/Na on the discharge curve at current densities equal to or below 100 mA g^{-1}. These plateaus are ascribed to sodiation–desodiation reactions of Sn. However, they almost disappear at ≥200 mA g^{-1} regardless of the electrolyte. This indicates that the slow kinetics of the sodiation reaction for Sn prevents its full sodiation.[25] In contrast, clear charge–discharge potential plateaus are observed at around 0.6 V vs. Na^+/Na corresponding to the reaction of P with Na at current densities up to 500 mA g^{-1}. The reactions of Sn_4P_3 were further evaluated from the differential capacity vs. potential (dQ/dV) profiles (Figure 4b, d, and f). During charging, the peaks at 0.58, 0.16, and 0.005 V vs. Na^+/Na are attributed to the phase transformation reactions P → Na_3P_{11}, Na_3P_{11} → Na_3P, and Na_xSn → $Na_{15}Sn_4$, respectively.[26–28] While a clear peak is not observed, the reaction Sn → Na_xSn should occur at around 0.08 V vs. Na^+/Na. During discharging (desodiation), four peaks are observed at 0.19, 0.4, 0.62, and 0.9 V vs. Na^+/Na, which are assigned to the reverse reactions, as shown in Figure S1. At low current densities of ≤100 mA g^{-1}, the peak intensity at 0.005 V vs. Na^+/Na increases following the order: Py1MOM > Py1MEM > Py13. In addition, a peak is observed with the Py1MEM-based electrolyte even at a current density of 200 mA g^{-1} (Figure S2). Although it is not distinctly observed in the Py1MOM-based electrolyte, we have confirmed the peak attributed to the reverse reaction at 0.2 V vs. Na^+/Na. Thus, the $Na_{15}Sn_4$ phase is formed up to 200 mA g^{-1} in the Py1MOM- and Py1MEM-based electrolytes. In regard to the reaction of P with Na^+, the peak at 0.62 V vs. Na^+/Na (Na_3P → Na_3P_{11}) during discharging in the Py1MOM- and Py1MEM-based electrolytes

is larger than that for the Py13-based one (Figure S3). These results suggest that the sodiation–desodiation reactions of Sn and P are promoted upon introduction of an ether group to the cation side-chain. After the 51th cycle (50 mA g^{-1}), the capacities were almost same regardless of the electrolytes as shown in Figure 3. However, profiles of charge-discharge and dQ/dV in Py1MOM-FSA were different: the peak at 0.62 V vs. Na^+/Na ($Na_3P \rightarrow Na_3P_{11}$) was larger than that in the other electrolytes (Figure S4). A larger contribution of sodiation/desodiation reaction of P rather than Sn enables faster charge-discharge because of the slow kinetics of the sodiation reaction for Sn. We consider this promotion of reaction acts an important role for improve the rate performance.

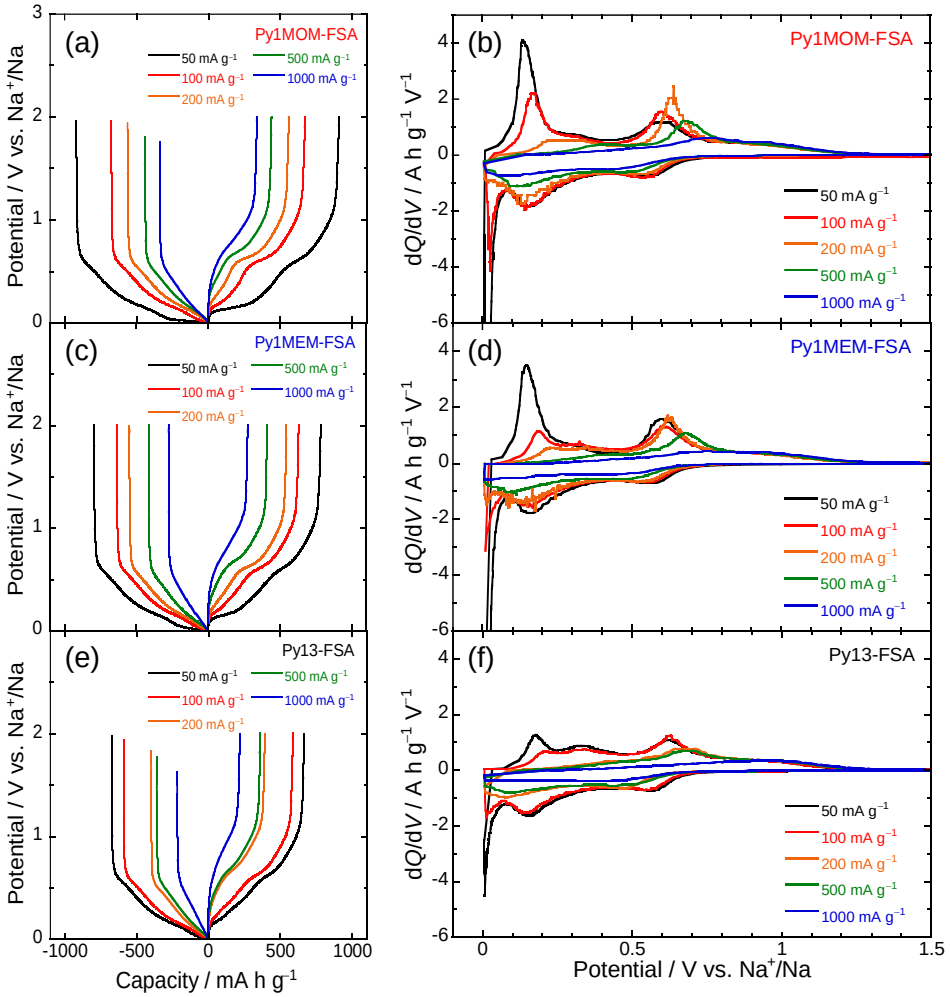

Figure 4 (a, c, e) Charge–discharge profiles and (b, d, f) dQ/dV curves for the Sn_4P_3 electrode in 1 M NaFSA-dissolved ionic liquid electrolytes of (a, b) Py1MOM-FSA, (c, d) Py1MEM-FSA, and (e, f) Py13-FSA under current densities ranging from 50 to 1000 mA g^{-1} at 303 K.

We have previously revealed that the electrochemical performance of a Si negative electrode for LIBs can be significantly improved by introducing an ether (MEM) group on the side-chain of the cation in ionic liquids.[19,29] This occurs because the MEM group reduces the electrostatic interactions between Li^+ and $TFSA^-$, thus promoting Li^+ transport at the electrode–electrolyte interface. In terms of NIBs, we assumed that the introduction of an ether group would also reduce the interaction between Na^+ and FSA^-, contributing to a higher rate capability. To analyze the solvation number of FSA^- per Na^+ cation, we prepared ionic liquid electrolytes with various concentrations of NaFSA, and performed Raman spectroscopy measurements. Figure S5 shows the Raman spectra of the ionic liquid electrolytes. The Raman band at ~728 cm^{-1} is attributed to the stretching vibration ν_s(S−N) of FSA^-.[30] The band indicates the presence of FSA^- not interacting with Na^+ (free FSA^-). An additional shoulder is observed at ~745 cm^{-1} with the increasing molar fraction of Na (Figure S6). Carstens *et al*. have reported that such a new band at ~743 cm^{-1} corresponds to the interaction between Na^+ and FSA^- (Na^+-FSA^-).[30] The solvation number was determined from said Raman band in the wavenumber range of 650–800 cm^{-1}. All Raman bands were deconvoluted into two components, those of free FSA^- and Na^+-FSA^-, using a Gaussian function, as shown in Figure 5a–c. The band intensity of Na^+-FSA^- ($I_{Na^+\text{-}FSA^-}$) in the Py1MEM-based electrolyte is significantly low, indicating that the MEM group reduces the electrostatic interactions between Na^+ and FSA^-. Plots of $I_{Na^+\text{-}FSA^-}/(I_{\text{free } FSA^-} + I_{Na^+\text{-}FSA^-})$ as a function of the molar fraction (x) of NaFSA for the different electrolyte solutions afforded a straight line (Figure 5d). This slope corresponds to the average solvation number of FSA^- per Na^+.[31,32] The average solvation number was calculated as 2.54 for the Py13-based electrolyte and 2.40 for the Py1MOM-based electrolyte. It has been reported that the solvation number of FSA^- per Na^+ is 2.7 in the electrolyte consisting of 1-butyl-1-methylpyrrolidinium

(Py14)-FSA.[30] It is suggested that both $[Na(FSA)_3]^{2-}$ and $[Na(FSA)_2]^-$ complexes exist in the electrolytes. Kunze *et al.* have reported that the solvation number of $TFSA^-$ per Li^+ in a Py13-based electrolyte was smaller than that in a Py14-based electrolyte.[33] This is caused by aggregation of the Py14 cations due to the stronger hydrophobic interactions between the long alkyl chains.[33] Thus, the solvation number in the Py13-based electrolyte is smaller than 2.7 in this study. The solvation number in the Py1MOM-based electrolyte is equal to or slightly lower than that for the Py13-based one. This might be because the oxygen atom in the MOM group acts repulsively against FSA^- minimizing the interaction between Na^+ and FSA^-. On the other hand, the solvation number was determined as 1.63 for the Py1MEM-based electrolyte, the lowest value of all the electrolytes. It is considered that the Py1MEM cation favors the Na^+ binding with FSA^- through the two oxygen atoms in its ether side-chain to form a Py1MEM–NaFSA complex, as is the case with the PP1MEM–LiTFSA complex we have previously reported.[29] Therefore, the average solvation number of FSA^- in the Py1MEM-based electrolyte is lower than that for the other electrolytes. A lower solvation number should contribute to improve the rate capability. However, the Sn_4P_3 electrode exhibits higher rate capability in the Py1MOM-based electrolyte than in the Py1MEM-based one. In addition, the reaction of Na^+ with Sn or P is promoted in the Py1MOM-based electrolyte compared to the Py13-based one, as shown in Figures 3 and 4. From these results, as expected, the introduction of an ether moiety in the short side-chains of the Py13 cation is a promising approach for NIBs to enhance the rate capability. If both reduced solvation number and improved conductivity can be realized, the rate capability may be further improved.

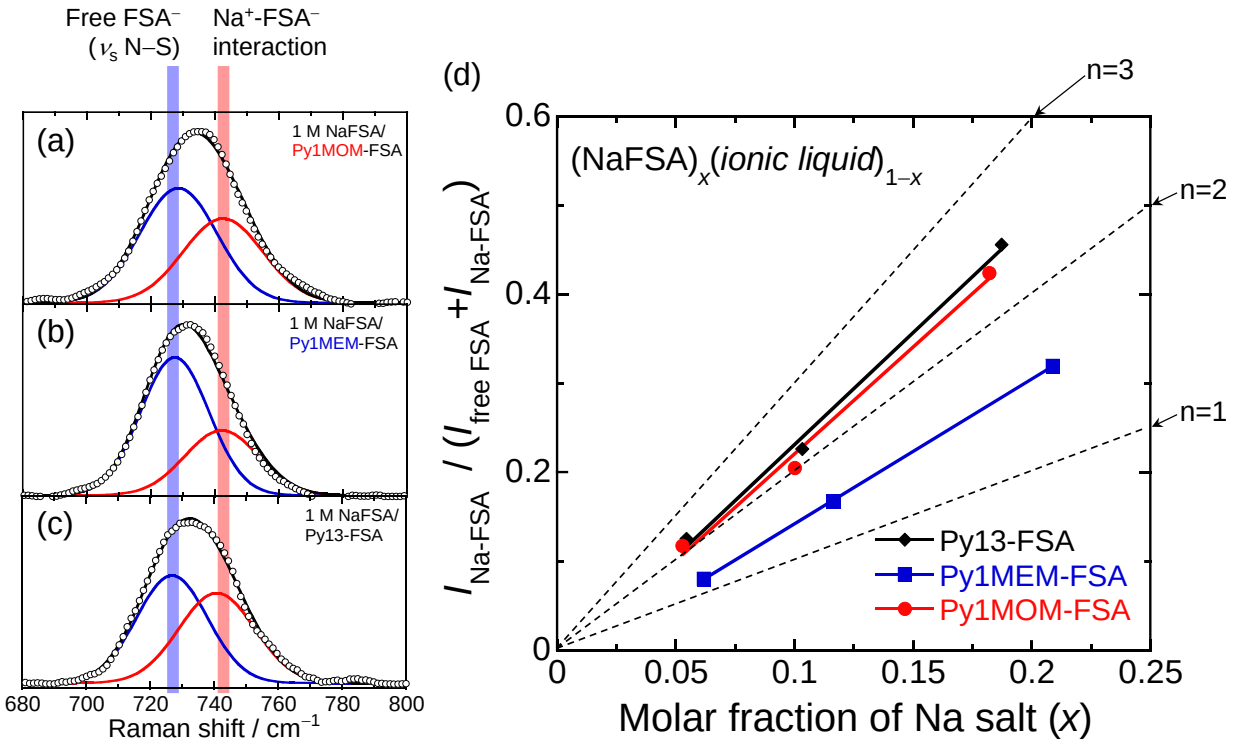

Figure 5 Deconvoluted Raman bands of 1 M NaFSA-dissolved in (a) Py1MOM-FSA, (b) Py1MEM-FSA, and (c) Py13-FSA. The dotted, black, blue, and red lines denote the recorded spectrum, total Raman spectrum, and deconvoluted components for free FSA and coordinated FSA (Na^+-FSA^-), respectively. (d) Plot of $I_{Na^+\text{-}FSA^-}/(I_{free\ FSA^-}+I_{Na^+\text{-}FSA^-})$ as a function of x for $(NaFSA)_x(Py13\text{-}FSA)_{1-x}$, $(NaFSA)_x(Py1MEM\text{-}FSA)_{1-x}$, and $(NaFSA)_x(Py1MOM\text{-}FSA)_{1-x}$. The dotted lines indicate the slopes for the cases where the average solvation numbers of FSA^- per Na^+ were 1, 2, and 3.

4. Conclusions

We have investigated the effect of the cation structure in ionic liquids on the electrochemical performance of the Sn_4P_3 negative electrode for NIBs. Ether-substituted ionic liquid electrolytes NaFSA/Py1MOM-FSA and NaFSA/Py1MEM-FSA successfully enhanced the rate capability of the electrode. The electrochemical reaction of Na^+ and Sn/P was promoted in these electrolytes compared to the Py13-based electrolyte without ether moieties, further contributing to a higher capacity. Introduction of an ether group in the side-chain of the ionic

liquid cation reduces the electrostatic interactions between Na^+ and FSA^- in the electrolyte; as a result, the solvation number of FSA^- per Na^+ is reduced, especially in the Py1MEM-based electrolyte. While the solvation number in the Py1MOM-based electrolyte was found to be greater than in the Py1MEM-based one, its conductivity was significantly higher, leading to better rate capability. Therefore, the introduction of an ether group in the short side-chains of the Py13 cation is a better approach to improve the conductivity and enhance the rate capability of the Sn_4P_3 electrode. Simultaneously, this strategy will be useful for improvement of NIBs and NICs.

Acknowledgement

This study has been partially supported by the Advanced Low Carbon Technology Research and Development Program (ALCA, 16200610802), Joint Usage/Research Program on Zero-Emission Energy Research, Institute of Advanced Energy, Kyoto University (ZE29A-14, ZE30A-05, ZE30A-06), and Japan Society for the Promotion of Science (JSPS) KAKENHI (Grant Number 17H03128, 17K17888, 16K05954). We would like to thank Editage (www.editage.jp) for English language editing.

References

[1] S. Komaba, W. Murata, T. Ishikawa, N. Yabuuchi, T. Ozeki, T. Nakayama, A. Ogata, K. Gotoh, K. Fujiwara, Electrochemical Na Insertion and Solid Electrolyte Interphase for Hard-Carbon Electrodes and Application to Na-Ion Batteries, Adv. Funct. Mater. 21 (2011) 3859–3867. doi:10.1002/adfm.201100854.

[2] G. Hasegawa, K. Kanamori, N. Kannari, J. Ozaki, K. Nakanishi, T. Abe, Studies on electrochemical sodium storage into hard carbons with binder-free monolithic electrodes, J. Power Sources. 318 (2016) 41–48. doi:10.1016/j.jpowsour.2016.04.013.

[3] H. Wang, C. Zhu, D. Chao, Q. Yan, H.J. Fan, Nonaqueous Hybrid Lithium-Ion and Sodium-Ion Capacitors, Adv. Mater. 29 (2017) 1702093. doi:10.1002/adma.201702093.

[4] Y. Li, H. Wang, L. Wang, Z. Mao, R. Wang, B. He, Y. Gong, X. Hu, Mesopore-Induced Ultrafast Na^+-Storage in T-Nb_2O_5/ Carbon Nanofiber Films toward Flexible High-Power Na-Ion Capacitors, Small. 15 (2019) 1804539. doi:10.1002/smll.201804539.

[5] S. Komaba, Y. Matsuura, T. Ishikawa, N. Yabuuchi, W. Murata, S. Kuze, Redox reaction of Sn-polyacrylate electrodes in aprotic Na cell, Electrochem. Commun. 21 (2012) 65–68. doi:10.1016/j.elecom.2012.05.017.

[6] M. Shimizu, H. Usui, K. Yamane, T. Sakata, T. Nokami, T. Itoh, H. Sakaguchi, Electrochemical Na-Insertion/Extraction Properties of Phosphorus Electrodes in Ionic Liquid Electrolytes, Int. J. Electrochem. Sci. 10 (2015) 10132–10144.

[7] A. Darwiche, C. Marino, M.T. Sougrati, B. Fraisse, L. Stievano, L. Monconduit, Better Cycling Performances of Bulk Sb in Na-Ion Batteries Compared to Li-Ion Systems: An Unexpected Electrochemical Mechanism, J. Am. Chem. Soc. 134 (2012) 20805–20811. doi:10.1021/ja310347x.

[8] M. Shimizu, H. Usui, K. Fujiwara, K. Yamane, H. Sakaguchi, Electrochemical behavior of SiO as an anode material for Na-ion battery, J. Alloys Compd. 640 (2015) 440–443. doi:10.1016/j.jallcom.2015.03.171.

[9] M. Shimizu, H. Usui, H. Sakaguchi, Electrochemical Na-insertion/extraction properties of SnO thick-film electrodes prepared by gas-deposition, J. Power Sources. 248 (2014) 378–382. doi:10.1016/j.jpowsour.2013.09.046.

[10] J. Qian, X. Wu, Y. Cao, X. Ai, H. Yang, High Capacity and Rate Capability of Amorphous Phosphorus for Sodium Ion Batteries, Angew. Chem. Int. Ed. 52 (2013) 4633–4636. doi:10.1002/anie.201209689.

[11] M. Shimizu, Y. Tsushima, S. Arai, Electrochemical Na-Insertion/Extraction Property of Ni-Coated Black Phosphorus Prepared by an Electroless Deposition Method, ACS Omega. 2 (2017) 4306–4315. doi:10.1021/acsomega.7b00950.

[12] H. Usui, T. Sakata, M. Shimizu, H. Sakaguchi, Electrochemical Na-insertion/Extraction Properties of Sn–P Anodes, Electrochemistry. 83 (2015) 810–812. doi:10.5796/electrochemistry.83.810.

[13] H. Usui, Y. Domi, K. Fujiwara, M. Shimizu, T. Yamamoto, T. Nohira, R. Hagiwara, H. Sakaguchi, Charge-Discharge Properties of a Sn_4P_3 Negative Electrode in Ionic Liquid Electrolyte for Na-Ion Batteries, ACS Energy Lett. 2 (2017) 1139–1143. doi:10.1021/acsenergylett.7b00252.

[14] H. Usui, Y. Domi, H. Nishida, K. Yamaguchi, R. Yamagami, H. Sakaguchi, Enhanced Performance of Sn_4P_3 Electrode Cycled in Ionic Liquid Electrolyte at Intermediate Temperature as Na-Ion Battery Anode, ChemistrySelect. 3 (2018) 8462–8467. doi:10.1002/slct.201801517.

[15] H. Usui, Y. Domi, R. Yamagami, K. Fujiwara, H. Nishida, H. Sakaguchi, Sodiation−Desodiation Reactions of Various Binary Phosphides as Novel Anode Materials of Na-Ion Battery, ACS Appl. Energy Mater. 1 (2018) 306–311. doi:10.1021/acsaem.7b00241.

[16] D. Monti, E. Jónsson, M.R. Palacín, P. Johansson, Ionic liquid based electrolytes for sodium-ion batteries: Na^+ solvation and ionic conductivity, J. Power Sources. 245 (2014) 630–636. doi:10.1016/j.jpowsour.2013.06.153.

[17] C.Y. Li, J. Patra, C.H. Yang, C.M. Tseng, S.B. Majumder, Q.F. Dong, J.K. Chang, Electrolyte Optimization for Enhancing Electrochemical Performance of Antimony Sulfide/Graphene Anodes for Sodium-Ion Batteries-Carbonate-Based and Ionic Liquid Electrolytes, ACS Sustainable Chem. Eng. 5 (2017) 8269–8276. doi:10.1021/acssuschemeng.7b01939.

[18] H. Usui, Y. Domi, M. Shimizu, A. Imoto, K. Yamaguchi, H. Sakaguchi, Niobium-doped titanium oxide anode and ionic liquid electrolyte for a safe sodium-ion battery, J. Power Sources. 329 (2016) 428–431. doi:10.1016/j.jpowsour.2016.08.049.

[19] M. Shimizu, H. Usui, K. Matsumoto, T. Nokami, T. Itoh, H. Sakaguchi, Effect of Cation Structure of Ionic Liquids on Anode Properties of Si Electrodes for LIB, J. Electrochem. Soc. 161 (2014) A1765–A1771. doi:10.1149/2.0021412jes.

[20] M. Montanino, M. Carewska, F. Alessandrini, S. Passerini, G.B. Appetecchi, The role of the cation aliphatic side chain length in piperidinium bis(trifluoromethansulfonyl)imide ionic liquids, Electrochim. Acta. 57 (2011) 153–159. doi:10.1016/j.electacta.2011.03.089.

[21] T. Nokami, K. Matsumoto, T. Itoh, Y. Fukaya, T. Itoh, Synthesis of Ionic Liquids Equipped with 2-Methoxyethoxymethyl/Methoxymethyl Groups Using a Simple Microreactor System, Org. Process Res. Dev. 18 (2014) 1367–1371. doi:10.1021/op500131u.

[22] K. Tsunashima, A. Kawabata, M. Matsumiya, S. Kodama, R. Enomoto, M. Sugiya, Y. Kunugi, Low viscous and highly conductive phosphonium ionic liquids based on bis(fluorosulfonyl)amide anion as potential electrolytes, Electrochem. Commun. 13 (2011) 178–181. doi:10.1016/j.elecom.2010.12.007.

[23] J. Qian, Y. Xiong, Y. Cao, X. Ai, H. Yang, Synergistic Na-storage reactions in Sn_4P_3 as a high-capacity, cycle-stable anode of Na-ion batteries, Nano Lett. 14 (2014) 1865–1869. doi:10.1021/nl404637q.

[24] Y. Kim, Y. Kim, A. Choi, S. Woo, D. Mok, N.S. Choi, Y.S. Jung, J.H. Ryu, S.M. Oh, K.T. Lee, Tin phosphide as a promising anode material for Na-ion batteries, Adv. Mater. 26 (2014) 4139–4144. doi:10.1002/adma.201305638.

[25] L. Baggetto, P. Ganesh, R.P. Meisner, R.R. Unocic, J.C. Jumas, C.A. Bridges, G.M. Veith, Characterization of sodium ion electrochemical reaction with tin anodes: Experiment and theory, J. Power Sources. 234 (2013) 48–59. doi:10.1016/j.jpowsour.2013.01.083.

[26] M. Mortazavi, Q. Ye, N. Birbilis, N. V. Medhekar, High capacity group-15 alloy anodes for Na-ion batteries: Electrochemical and mechanical insights, J. Power Sources. 285 (2015) 29–36. doi:10.1016/j.jpowsour.2015.03.051.

[27] J.M. Sangster, Na-P (Sodium-Phosphorus) System, J Phase Equilib. Diff. 31 (2010) 62–67. doi:10.1007/s11669-009-9613-z.

[28] Z. Du, R.A. Dunlap, M.N. Obrovac, Investigation of the reversible sodiation of Sn foil by ex-situ X-ray diffractometry and Mössbauer effect spectroscopy, J. Alloys Compd. 617 (2014) 271–276. doi:10.1016/j.jallcom.2014.07.209.

[29] M. Shimizu, H. Usui, H. Sakaguchi, Functional ionic liquids for enhancement of Li-ion transfer: the effect of cation structure on the charge-discharge performance of the $Li_4Ti_5O_{12}$ electrode, Phys. Chem. Chem. Phys. 18 (2016) 5139–5147. doi:10.1039/C5CP05008A.

[30] T. Carstens, A. Lahiri, N. Borisenko, F. Endres, $[Py_{1,4}]$FSI-NaFSI-based ionic liquid electrolyte for sodium batteries: Na^+ solvation and interfacial nanostructure on Au(111), J. Phys. Chem. C. 120 (2016) 14736–14741. doi:10.1021/acs.jpcc.6b04729.

[31] S. Menne, T. Vogl, A. Balducci, Lithium coordination in protic ionic liquids, Phys. Chem. Chem. Phys. 16 (2014) 5485–5489. doi:10.1039/c3cp55183k.

[32] S. Duluard, J. Grondin, J.-L.L. Bruneel, I. Pianet, A. Grélard, G. Campet, M.-H.H. Delville, J.-C. Lassègues, Lithium solvation and diffusion in the 1-butyl-3-methylimidazolium bis(trifluoromethanesulfonyl)imide ionic liquid, J. Raman Spectrosc. 39 (2008) 627–632. doi:10.1002/jrs.1896.

[33] M. Kunze, S. Jeong, E. Paillard, M. Schönhoff, M. Winter, S. Passerini, New insights to self-aggregation in ionic liquid electrolytes for high-energy electrochemical devices, Adv. Energy Mater. 1 (2011) 274–281. doi:10.1002/aenm.201000052.